Vortex-antivortex lattices in a holographic superconductor

Jia-Hao Su,[1] Chuan-Yin Xia,[1] Wei-Can Yang,[1,3] and Hua-Bi Zeng[1,2,*]

[1]*Center for Gravitation and Cosmology, College of Physical Science and Technology, Yangzhou University, Yangzhou 225009, China*

[2]*Center for Theoretical Physics, Hainan University, Haikou 570228, China*

[3]*Department of Physics, Osaka Metropolitan University, 3-3-138 Sugimoto, 558-8585 Osaka, Japan*

(Received 20 November 2023; accepted 2 February 2024; published 28 February 2024)

We employ the Einstein-Abelian-Higgs theory to investigate the structure of vortex-antivortex lattices within a superconductor driven by spatial periodic magnetic fields. By adjusting the parameters of the external magnetic field, including the period ($\mathcal{T}$) and the amplitude (B_0), various distinct vortex states emerge. These states encompass the Wigner crystallization state, the vortex cluster state, and the suppressed state. Additionally, we present a comprehensive phase diagram to demarcate the specific regions where these structures emerge, contributing to our understanding of superconductivity in complex magnetic environments.

DOI: 10.1103/PhysRevD.109.046019

I. INTRODUCTION

Type II superconductors are a distinct class of superconducting materials characterized by higher critical fields and stronger diamagnetism compared to type I superconductors [1–5]. The type of superconductor can be determined by the characteristic parameter $\kappa = \lambda/\xi$, which is defined as the ratio of the magnetic penetration depth (λ) to the coherence length of the order parameter (ξ). When $\kappa < \frac{1}{\sqrt{2}}$, the interface energy between the superconducting and normal states is positive, resulting in diamagnetism and classifying it as a type I superconductor. On the other hand, when $\kappa > \frac{1}{\sqrt{2}}$, the interface energy is negative, resulting in the formation of the mixed state [6–13], i.e., the normal state occurs as vortices emerge on the superconductor to maintain a minimal free energy, which characterizes the type II superconductor.

Specifically, upon the application of a weak, uniform magnetic field to a superconductor, diamagnetic surface currents are induced inside the superconductor because of the presence of an external field outside the superconductor-vacuum interface. The penetration of the magnetic field within the superconductor follows the expression $B(x) \sim B_0 e^{-x/\lambda}$, where B_0 is the external magnetic field and x is the direction perpendicular to the interface, magnetic fields decay exponentially inside the superconductor; this can be obtained from the London equation. This phenomenon is known as the Meissner effect. When the magnetic field increases to a critical point, the superconductor and magnetic field "meet a compromise", forming Abrikosov vortices, which can be arranged as triangular or square lattices [14–18].

Unlike the effects of a uniform magnetic field, the application of a periodic magnetic field to a superconductor gives rise to a more diverse range of phenomena, notably the emergence of vortex-antivortex pairs. These phenomena have been extensively studied in nonlinear time-dependent Ginzburg-Landau (TDGL) theory, yielding a wealth of insight [19–24]. Nonetheless, the study of magnetic fields in strongly coupled superconductors is constrained by the limitations of the TDGL equation. Therefore, the exploration of such systems necessitates the utilization of alternative theoretical tools or approaches. Recently, it became possible to address magnetic field effect in strongly coupled type II superconductor using holographic duality discovered in string theory, mapping a superconductor to a gravitational theory in one higher dimension with a charged scalar living in the bulk [25–29]. The charged scalar field represents the superconducting order parameter in dual field theory, and its condensation leads to the formation of a superconducting phase. The scalar can have a nonzero profile with lower free energy than the trivial zero solution when the temperature of the black hole is low enough [29]. Furthermore, the holographic works [30–34] found that the holographic model shares numerous similarities with the TDGL equations and extends beyond their scope. In [35–37], it was demonstrated that the model indeed corresponds to superfluid hydrodynamics. Previous studies have investigated the

*hbzeng@yzu.edu.cn

formation of a vortex lattice in a rotating holographic superfluid [38–40], as well as the effects of an external magnetic field in the holographic superconductor model [41–44]. Otherwise, excitation with dynamical Maxwell fields at the boundary has also been explored in [45–47]. The single vortex solution [48–51], vortex lattice solution [52–54] under the magnetic field, and a periodic solution called the holographic checkerboard [55,56] have already been obtained. Notably, all these previous studies have focused primarily on the effects of a uniform magnetic field; thus, how the periodic magnetic field affects the holographic superconductivity is a problem worth exploring.

In this research, we conducted an in-depth analysis of vortex-antivortex lattices within a holographic superconducting film subjected to a periodic magnetized field. Once the period number surpasses a specific threshold, the vortex and antivortex will annihilate each other, resulting in a magnetic field of zero throughout. Consequently, the Meissner state can be maintained regardless of the value of B_0, unless an excessively strong magnetic field completely disrupts the superconducting state. If the period number is kept within a suitable range, as the magnetic strength increases, the superconductor will go through the Meissner state, vortex state (including Wigner crystallization with rotational symmetry and vortex clusters with mirror symmetry), suppressed state, and eventually the normal state. It is worth noting that, in the context of our study, we also discovered that at a critical magnetic field strength, vortex-antivortex pairs begin to proliferate, forming larger clusters. This phenomenon leads to the emergence of long-range order within the system.

The paper is organized as follows. In Sec. II, we introduce the holographic model and illustrate our setup, including the necessary theoretical framework and methodologies. In Sec. III, we show various configurations of vortex-antivortex lattices in a superconducting film with an external periodic magnetic field and explore the dynamics of these lattices within the film. In Sec. IV, we show the phase diagram taking the period $\mathcal{T}$ and the strength of the external magnetic field B_0 as variables. This phase diagram provides a visual representation of the different phases and states exhibited by the superconducting film under varying conditions. We summarize our results in Sec. V.

II. HOLOGRAPHIC MODEL

In $(3+1)$-dimensional anti–de Sitter (AdS) space-time, we adopted a holographic superconducting model with a gauge field and a complex scalar field in the presence of a planar Schwarzschild black hole. This model is dual to a $(2+1)$-dimensional conformal field theory on the boundary. The action [28,29,57,58] can be expressed as

$$S(\Psi,A_\mu)=\frac{1}{16\pi G_N}\int d^4x\sqrt{-g}\left[\mathcal{R}+\frac{6}{L^2}+\frac{1}{q^2}\mathcal{L}_{\text{matter}}(\Psi,A_\mu)\right] \tag{1}$$

in which a complex scalar field Ψ is coupled to a U(1) gauge field A_μ in $(3+1)$D gravity with a cosmological constant related to the AdS radius as $\Lambda=-3/L^2$. The G_N is the gravitational constant, we set $16\pi G_N=1$. The first two terms in parentheses are the gravitational part of the Lagrangian with the Ricci scalar $\mathcal{R}$, and the radius of the AdS spacetime L. The Lagrangian matter field is

$$\mathcal{L}_{\text{matter}}(\Psi,A_\mu)=-\frac{1}{4}F_{\mu\nu}F^{\mu\nu}-|D_\mu\Psi|^2-m^2|\Psi|^2, \tag{2}$$

where $F_{\mu\nu}=\partial_\mu A_\nu-\partial_\nu A_\mu$ is the component of the $U(1)$ gauge field and Ψ is the complex scalar field with mass m. D_μ is the covariant derivative written as $D_\mu\Psi=\partial_\mu\Psi-iq_sA_\mu\Psi$ with the charge of the scalar field, as a Cooper pair, $q_s=2\text{e}$. We work in the probe limit by taking the $q\to\infty$, which means that the matter fields decouple from gravity, so standard Schwarzschild-AdS black brane to provide a constant temperature with metric,

$$ds^2=\frac{l^2}{z^2}(-f(z)dt^2-2dtdz+dx^2+dy^2), \tag{3}$$

where $z=0$ represents the AdS boundary and $z=z_h$ is the horizon of black hole. Without loss of generality, we can set $z_h=L=1$, then $f(z)=1-z^3$, and the Hawking temperature can be written as $T=3/4\pi$.

With the action one can obtain the equation of motion for the scalar field

$$D^\mu D_\mu\Psi-m_s^2\Psi=0, \tag{4}$$

and the equation of motion for the vector field

$$\partial^\nu F_{\nu\mu}-iq_s(\Psi^*D_\mu\Psi-\Psi D_\mu\Psi^*)=0. \tag{5}$$

A trivial solution with $\Psi=0$ can be easily obtained from the equation mentioned above. However, when the potential on the AdS boundary is increased beyond a critical value, a nonzero solution for the scalar field appears. This indicates that for temperatures below T_c, a charged scalar operator has condensed, leading to the breaking of U(1) symmetry and the emergence of superconductivity.

The conformal dimensions of the scalar field can be obtained by setting $m_s^2=-2$, which yields $\Delta=\frac{3}{2}\pm\sqrt{\frac{9}{4}-m^2L^2}=\frac{3}{2}\pm\frac{1}{2}$. Therefore, the expansion of the scalar field solution near the AdS boundary takes the form of

$$\Psi=\phi z+\psi z^2+\mathcal{O}(z^3), \tag{6}$$

where $\phi|_{z=0}$ is set to be zero as a boundary condition when solving the model. Similarly, the gauge field near the AdS boundary can be expressed as

$$A_\nu = a_\nu + b_\nu z + \mathcal{O}(z^2), \tag{7}$$

where $a_t = \mu$ represents the chemical potential when $A_t(z_h) = 0$. If the value of μ exceeds a critical value $\mu_c = 4.07$, the U(1) gauge symmetry of the system is spontaneously broken, resulting in a finite-valued solution for the expectation value of the scalar operator $\langle O \rangle = \partial_z \psi$. From holographic renormalization [59], we can add the counterterms of the scalar fields,

$$S_{c.t.} = \int d^3x \sqrt{-\gamma} \Psi^* \Psi \tag{8}$$

into the divergent on shell action, where γ is the determinant of the reduced metric on the $z \to 0$ boundary. To obtain the dynamical gauge fields on the boundary, we impose the Neumann boundary conditions for the gauge fields as $z \to 0$ [60,61]. Thus, the surface term

$$S_{\text{surf}} = \int d^3x \sqrt{-\gamma} n^\mu F_{\mu\nu} A^\nu \tag{9}$$

near the boundary should be added as well in order to have a well-defined variation, where n^μ is the normal vector perpendicular to the boundary. Hence, we obtain the finite renormalized on shell action S_{ren}. Therefore, the expectation value of the order parameter, $\langle O \rangle = \Psi_1$, can be obtained by varying S_{ren} with respect to Ψ_0. Expanding the z-component of the Maxwell equations near the boundary we get $\partial_t b_t + \partial_i J^i = 0$, which is exactly a conservation equation of the charge density and current on the boundary since from the variation of S_{ren} one can easily deduce that $b_t = -\rho$ with ρ the charge density and $J^i = -b_i - (\partial_i a_t - \partial_t a_i)$ (which is the i-direction current), respectively. In the Eddington coordinate, the current j_μ is related to b_μ through $j_\mu = -b_\mu - \partial_\mu a_t + \partial_t a_\mu$ and the temperature T is related to μ through $T = (\mu_c/\mu) T_c$, following the holographic dictionary. In the case of a superconductor, the Neumann boundary condition for A_x and A_y is fixed as $j_x = j_y = 0$ in $z = 0$.

In order to apply an external periodic magnetic field to the superconducting film at $t = 0$, we turn to

$$A_x = A_0 \sin\left(\mathcal{T} \frac{y\pi}{l}\right), \tag{10}$$

$$A_y = -A_0 \sin\left(\mathcal{T} \frac{x\pi}{l}\right), \tag{11}$$

where $\mathcal{T}$ represents the period number and l represents the size of superconductor. The magnetic field can be obtained by taking the curvature of the vector potential A using the equation $B = \nabla \times A$. In two dimensions, this equation can be expressed as

$$B = -B_0 \left[\cos\left(\mathcal{T} \frac{x\pi}{l}\right) + \cos\left(\mathcal{T} \frac{y\pi}{l}\right)\right], \tag{12}$$

where $B_0 = A_0 \mathcal{T} \pi / l$. A periodic magnetic field can be generated experimentally by arranging cubic magnetic dots in an array. This allows researchers to study superconductor film directly in a controlled and repeatable way with periodic magnetic field [62–64].

For the numerical simulation, the Chebyshev spectral is used in the z-direction with 30 points. Fourier spectral is used in the (x, y)-direction with 200×200 points. The evolution of time is simulated by the fourth-order Runge-Kutta method. The initial configuration at $t = 0$ is chosen to be a superconducting state at fixed $l = 50$ and $\mu = 10$, so temperature $T = 0.407 T_c$.

III. THE PATTERNS OF VORTEX-ANTIVORTEX LATTICES

This study investigates the consequences of introducing an external periodic magnetic field to a superconductor. This leads to the formation of various patterns of vortex-antivortex lattices. Similar to the experimental setup for generating vortices, we prepare a homogeneous superconducting state as the initial configuration, where the boundary condition is adjusted to introduce a periodic magnetic field onto the superconductor, resulting in system driving. To intuitively understand this, it can be considered as a regular cubic array of magnetic dots on the superconductor film. This cubic symmetry allows us to gain insight into the behavior of the system when exposed to external magnetic fields. The density of the array is correlated with the period number. As the period number increases, the array contains more magnetic dots, leading to a higher density. On the contrary, a smaller period number results in a lower density of magnetic dots in the array. The density of the array is a major factor in determining the system's overall behavior and characteristics. There are several physical effects that cause patterns to form, such as matching effects with ordered pinning arrays, which add to the pinning force due to the magnetic properties of the pinning centers.

As A_0 increases, the process of a superconducting film can be described in four stages; the Meissner state, the vortex state including Wigner crystallization morphology and the vortex cluster morphology, the suppressed state, and the normal state. We examine two types of type II superconductor patterns; vortex-antivortex pairs lattice and suppressed patterns. Our study delves into the phase transition between vortex pairs and suppressed states, as well as the transition to the Meissner or normal state. The paper analyzes superconductor instabilities under a

magnetic field in a holographic model, where checkerboard order and periodic lattice states of vortex-antivortex pairs have been observed previously in the GL theory.

In Figs. 1–4, we show the vortex state patterns of the superconducting film, these patterns formed by the vortex-antivortex pairs exhibit various types of symmetry, including rotational symmetry, which can be expressed as an element of the group $SO(2)$ in the form of a matrix,

$$R(\pi/4) = \begin{bmatrix} 0 & -1 \\ 1 & 0 \end{bmatrix}.$$

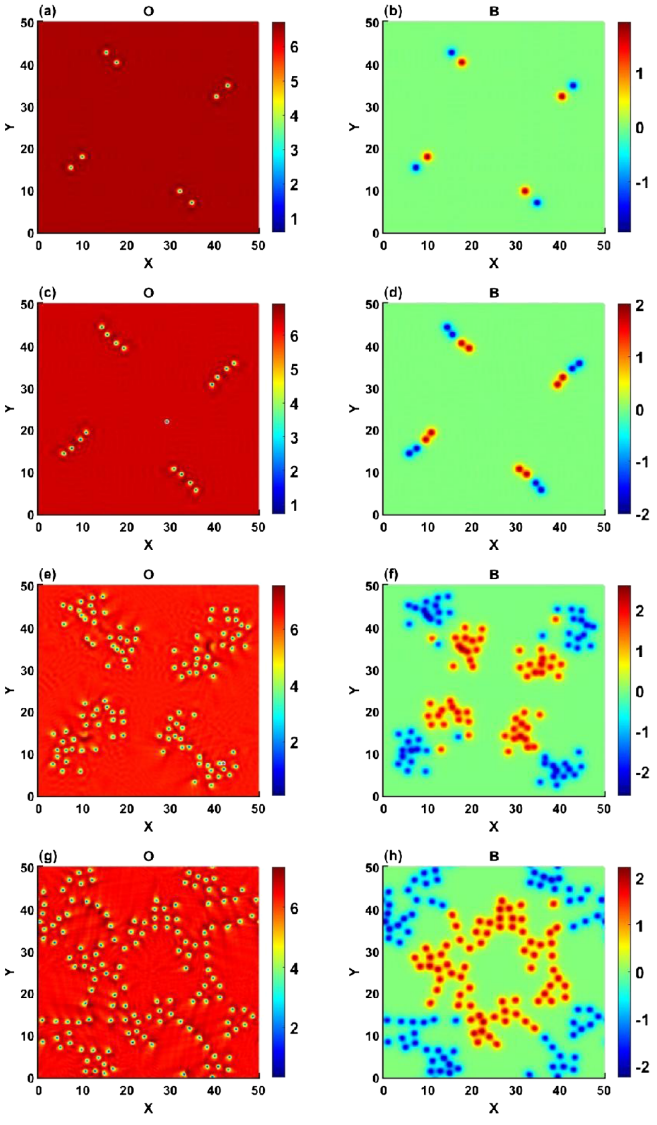

FIG. 1. Order parameter (left panels) and magnetic field (right panels) when (a),(b) $B_0 = 1.0304$, (c),(d) $B_0 = 1.0556$, (e),(f) $B_0 = 1.3195$, and (g),(h) $B_0 = 2.9531$. The order parameter is defined as $\langle O \rangle = \partial_z \Psi$, the magnetic field is defined as $B = \partial_x A_y - \partial_y A_x$. In this situation, with a magnetic period $\mathcal{T} = 2$, it can be considered as a primitive cell. The temperature $T = 0.407 T_c$.

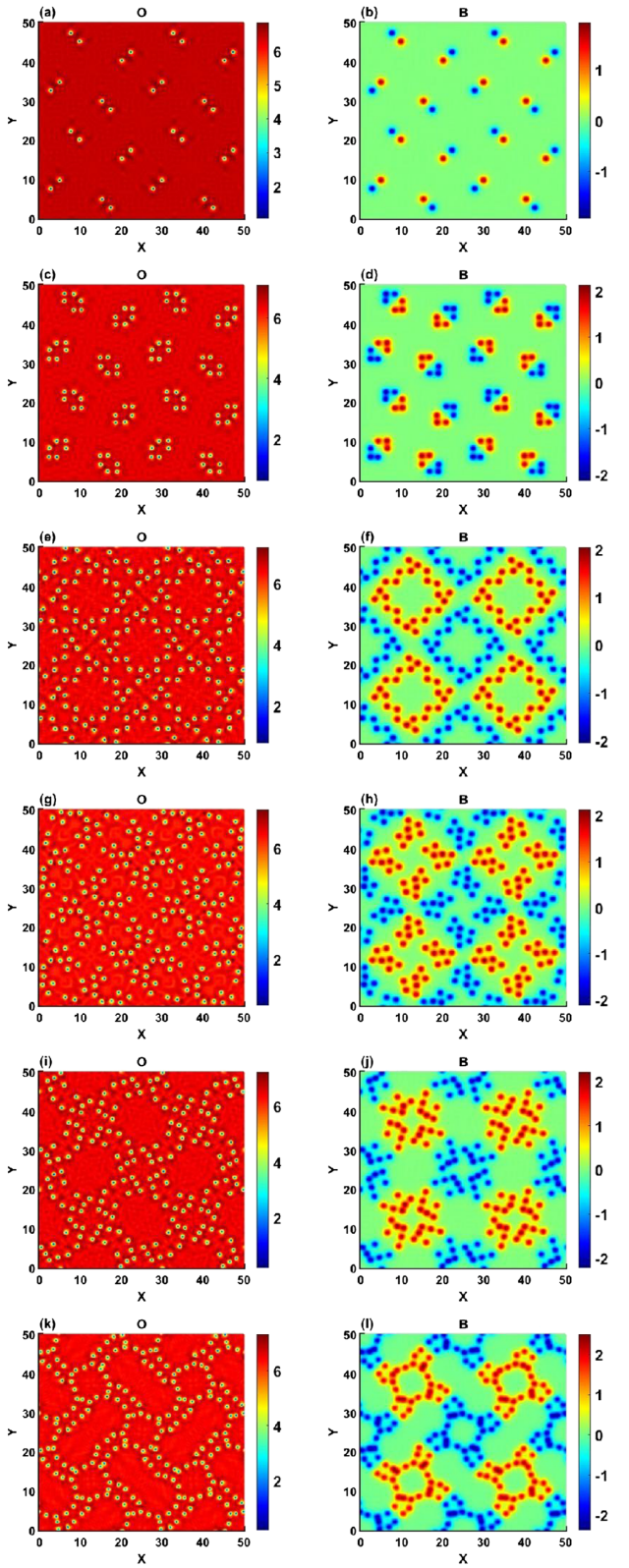

FIG. 2. Order parameter (left panels) and magnetic field (right panels) when (a),(b) $B_0 = 2.0609$, (c),(d) $B_0 = 2.2117$, (e),(f) $B_0 = 3.5186$, (g),(h) $B_0 = 4.0212$, (i),(j) $B_0 = 6.2832$, and (k),(l) $B_0 = 8.5451$. The temperature $T = 0.407 T_c$ and the magnetic period $\mathcal{T} = 4$.

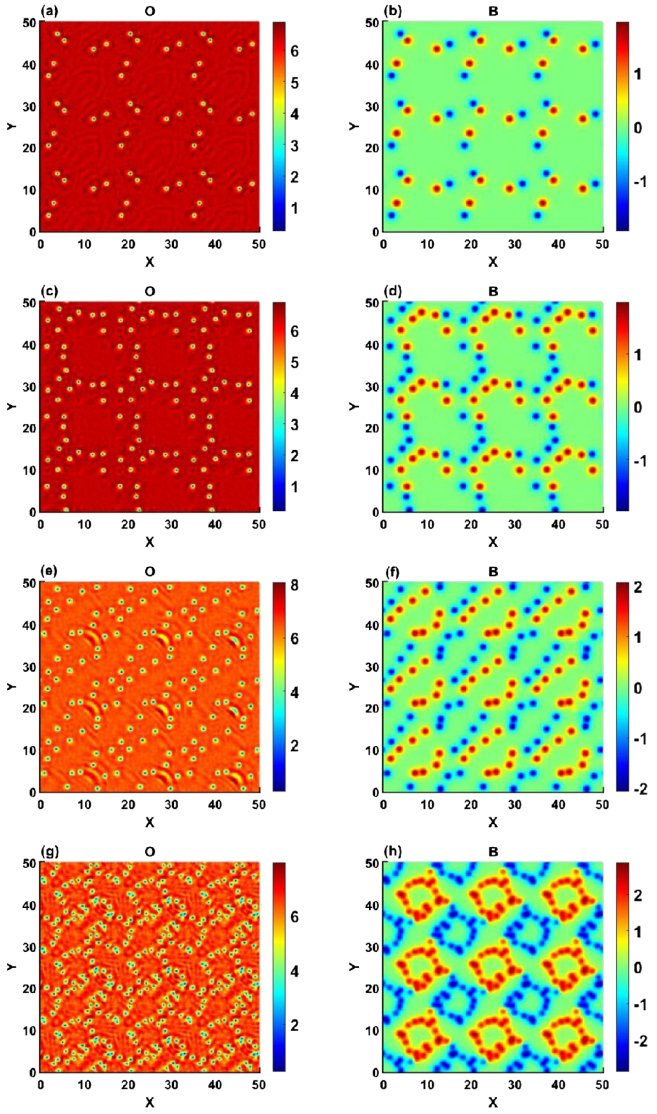

FIG. 3. Order parameter (left panels) and magnetic field (right panels) when (a),(b) $B_0 = 3.7699$, (c),(d) $B_0 = 4.9009$, (e),(f) $B_0 = 5.2779$, (g),(h) $B_0 = 5.6549$, and (i),(j) $B_0 = 11.3097$. The temperature $T = 0.407T_c$ and the magnetic period $\mathcal{T} = 6$.

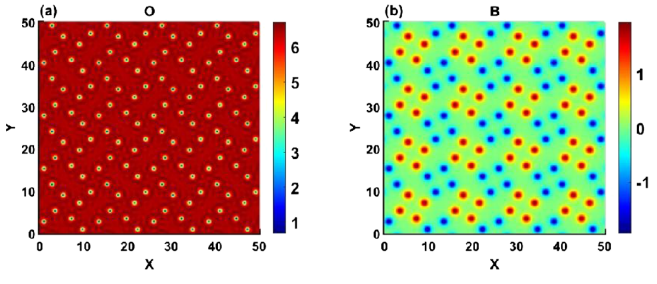

FIG. 4. Order parameter (left panels) and magnetic field (right panels) when (a),(b) $B_0 = 7.0372$. The temperature $T = 0.407T_c$ and the magnetic period $\mathcal{T} = 8$.

Additionally, the vortex cluster and antivortex cluster exhibit mirror symmetry form the vortex-antivortex cluster pair, which can be expressed as the equation $MX(x) = X(Mx)$, where M represents the mirror symmetry operation and $X(x)$ represents the position of the vortex. Furthermore, the patterns display transitional symmetry in some situations, suggesting the Wigner crystallization property. In normal cases, the entire pattern can be obtained through symmetry operations. Starting with a vortex cluster, applying the mirror symmetry operation results in a vortex-antivortex cluster pair. By rotating this cluster pair, a primitive cell is obtained. Finally, by translating this primitive cell, the entire pattern can be generated.

We choose even period numbers to maintain a zero total flux passing through the superconductor film. This choice ensures that there is an equal number of vortex and antivortex, thereby preserving the symmetry in the patterns of vortex-antivortex pairs. The patterns of $\mathcal{T} = 2$ can be regarded as a single positive magnetic dot that acts in the center of the film, and thus can be treated as a primitive cell, specifically a 1×1 crystal lattice, as depicted in Fig. 1. Due to the positive magnetic dot being pinned to provide positive flux on the film center, when the magnetization reaches a sufficient level, the negative flux near the magnetic dot induces the magnetic field lines to "join" and form antivortices. Since the total flux must remain zero, the emergence of vortex-antivortex pairs occurs near the magnetic dot. When $\mathcal{T} = 4$, as shown in Fig. 2, the patterns exhibit translation symmetry. Patterns can be identified as 2×2 crystal lattices. This situation can be interpreted as an array formed by four magnetic dots acting on the film. Around each magnetic dot, several vortex-antivortex pairs will form, resulting in the creation of vortex clusters, These vortex clusters represent a repeating units. The entire pattern observed in the superconducting film can always be obtained by translating a vortex cluster. Therefore, primitive cells can be associated with each magnetic dot. As the same way, the patterns of $\mathcal{T} = 6$ shown in Fig. 3 could be regarded as a 3×3 crystal lattice formed by an array of nine magnetic dots acting on the film. Similarly, the patterns of $\mathcal{T} = 8$ shown in Fig. 4 could be regarded as a crystal lattice of 4×4 formed by an array of sixteen magnetic dots acting on the film. In each case, the patterns induce transitional symmetry, suggesting the Wigner crystallization property. Not that, when $\mathcal{T} = 6$, the primitive cells do not exhibit rotational symmetry, so the entire pattern does not have rotational symmetry. The reason could be that the number of primitive cells is odd. In crystal lattices with an odd number of primitive cells, there is no equivalent rotation that can map one primitive cell onto another.

There is a special situation observed in Figs. 1(e)–(h), it is indeed observed that, when the system becomes very complex, the strict maintenance of symmetry becomes challenging due to the free evolution process of the system.

When the system reaches a certain level of complexity, the interactions between the vortex-antivortex pairs become intricate. The presence of multiple factors, such as the density and arrangement of the pairs, their motion and dynamics, and the influence of thermal fluctuations, contribute to the intricate behavior observed in the system. The complex interplay of various factors leads to deviations from idealized symmetrical patterns. Understanding and characterizing the complexity that arises from the interactions of vortex-antivortex pairs and thermal fluctuations is a challenging task in superconductivity research [65].

What is the cause of the complexity of the patterns increasing as the magnetic field strength increases when $\mathcal{T} = 2$, but increasing initially and then stabilizing in a region when $\mathcal{T} = 4,\ 6,\ 8$? The answer is that when $\mathcal{T} = 4, 6, 8$, there are multiple magnetic dots on the superconducting film, the vortex-antivortex pairs only can generate between the magnetic dots, the narrow area limits the complexity of the system as the vortex-antivortex pairs interact with each other. As the strength of the magnetic field increases, the area that can accommodate the vortex between the magnetic dots is restricted because the size of the area of influence of the magnetic dots also increases. So we can see the complexity of Figs. 2 and 3 rise first then down as increasing magnetic field, and the film is Meissner state when $\mathcal{T} = 8$, $A_0 = 20$, i.e., $B_0 = 10.0531$. However, when $\mathcal{T} = 2$, there is only one magnetic dot on the film, allowing the formation of multiple vortex-antivortex pairs. Sufficient area and strong magnetic strength induce the generation of large number pairs, that increases the complexity of the system. The system's complexity increases as more pairs are formed, creating intricate patterns. When $\mathcal{T} = 4, 6, 8$, the magnetic dots are arranged in a homogeneous alignment on the film and vortex-antivortex pairs are generated in the gap. The size of the magnetic dots is fixed and directly linked to the magnetization, so the system reaches a point where the number of pairs begins to decrease as the magnetization increases, even though it is theoretically expected that a higher magnetization will lead to more pairs as a result of the more prominent fluctuations in the superconducting film. This can be explained as follows. As the size of the magnetic dots "expands" due to a stronger magnetization, the available space for the formation of pairs is limited. This restriction on pair formation keeps the system's complexity in check, even when the magnetic field strength is higher.

When the strength of magnetic field applied to the superconductor film reaches a certain threshold, a new state shown in Fig. 5 emerges that the order parameter of the superconducting film is suppressed. This state is referred to as a metastable state because it can persist for a significant duration before transitioning back to either the vortex state or the superconducting state. The system returns to the vortex state shown in Fig. 6, it is a special case only when $\mathcal{T} = 2$. And when $\mathcal{T} = 4, 6, 8$, the system

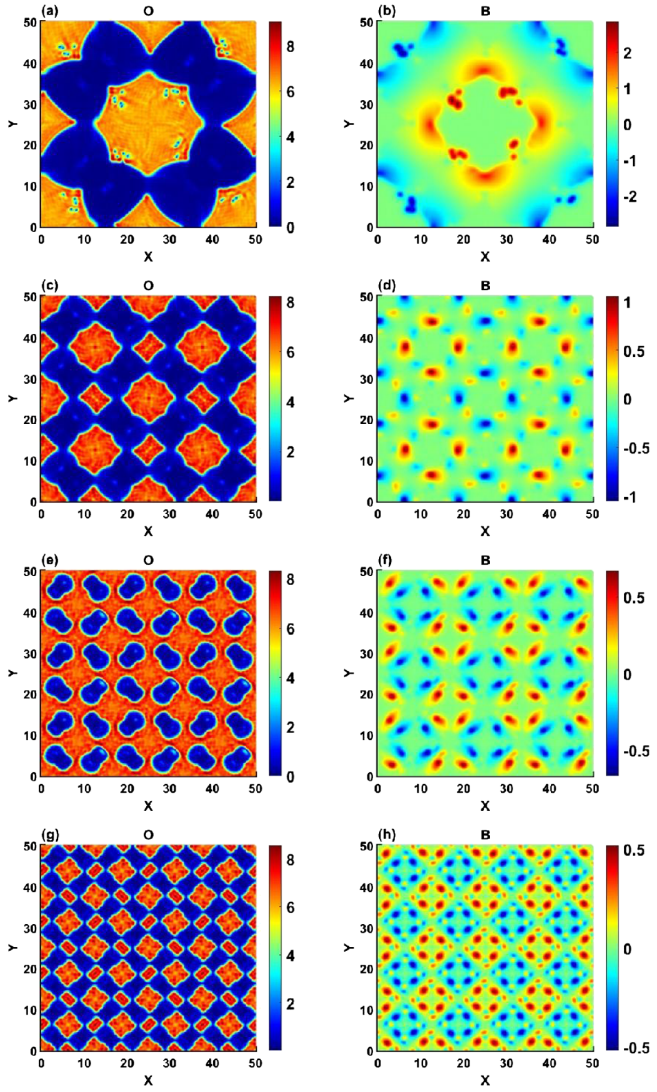

FIG. 5. Order parameter (left panels) and magnetic field (right panels) when (a),(b) magnetic period $\mathcal{T} = 2$ and $B_0 = 4.7752$, (c),(d) magnetic period $\mathcal{T} = 4$ and $B_0 = 9.5504$, (e),(f) magnetic period $\mathcal{T} = 6$ and $B_0 = 14.3257$, and (g),(h) magnetic period $\mathcal{T} = 8$ and $B_0 = 19.1009$. The temperature $T = 0.407T_c$ and the vector potential $A_0 = 38$.

reverts to the Meissner state. These situations also can be explained by considering the periodic magnetic field as a square array of submicrometer cubic magnetic dots with perpendicular magnetization. As was mentioned above, as the magnetic field strength increases, the size of the influence of magnetic dots also grows, resulting in a smaller gap between them. Consequently, although the system has a tendency to generate vortex-antivortex pairs, the reduced gap between the magnetic dots causes the pairs to cluster closely together, resulting in annihilation when $\mathcal{T} = 4, 6, 8$. This phenomenon only occurs when the magnetic field strength is relatively strong, and the specific properties of the magnetic dots lead to a cancellation of the magnetic field across the entire superconducting film.

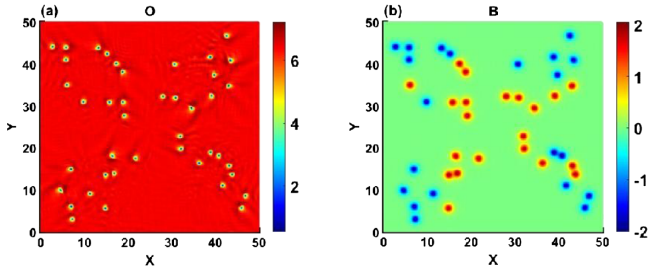

FIG. 6. Order parameter (left panels) and magnetic field (right panels) when the temperature $T = 0.406T_c$, the vector potential $A_0 = 38$, and magnetic field $B_0 = 4.7752$ and the magnetic period $\mathcal{T} = 2$. Suppressed state back to vortex state.

In Fig. 6, for $\mathcal{T} = 2$ and $A_0 = 38$ (i.e., $B_0 = 4.7752$), where only one magnetic dot interacts with the film, vortex pairs are not constrained to narrow gaps between magnetic dots, allowing the vortex state to persist. The dynamic transitions from the suppressed state back to the superconducting state due to vortex annihilation, and from the suppressed state back to the vortex state, are illustrated in a movie provided in the Supplementary Material [66].

IV. THE PHASE DIAGRAM

We have already shown that type II superconductors exhibit different types of phases under a periodic magnetic field, including the Meissner state, the vortex lattice state, the suppressed superconductivity state, and the normal state, as depicted in Fig. 7. On the basis of the phase diagram, the basic physical landscape could be described. When $\mathcal{T} < 8$, magnetization is too week in the cyan zone, so the magnetic field cannot enter the superconductor, as the magnetization gets stronger, the superconductor enters the vortex state and the quantity of vortex increases as B_0 increases. When the magnetic field strength increases to a critical value between the cyan zone and the magenta zone for a fixed $\mathcal{T}$, the superconductor transitions to the suppressed state, where the order parameter is suppressed due to the influence of a strong magnetic field on the superconducting film. Note that as $\mathcal{T}$ increases, the slope of the dividing line between different phases increases. To comprehend this behavior, we use a helpful analogy of the periodic magnetic field acting on the superconductor film as a regular array of cubic magnetic dots acting on the film. As the magnetic period number $\mathcal{T}$ increases, the density of these magnetic dot arrays also increases on the film. The increased density of magnetic dot array provides additional stability to the vortex state, making it less susceptible to suppression by the external magnetic field. The emerge of suppressed state and its evolution progress is interesting, the phenomenon and the progress including rich dynamic procedure between order parameter and magnetic field. Then as B_0 continue increases to a critical value between yellow zone and green zone for a fixed $\mathcal{T}$, the superconductor is completely destroyed by magnetic field. The situation of $\mathcal{T} > 8$ is special, the density of the magnetic dot array is too high, resulting in a gap between two dots that is too small. This causes vortex annihilation before the system can become stable, leaving only superconducting and normal states.

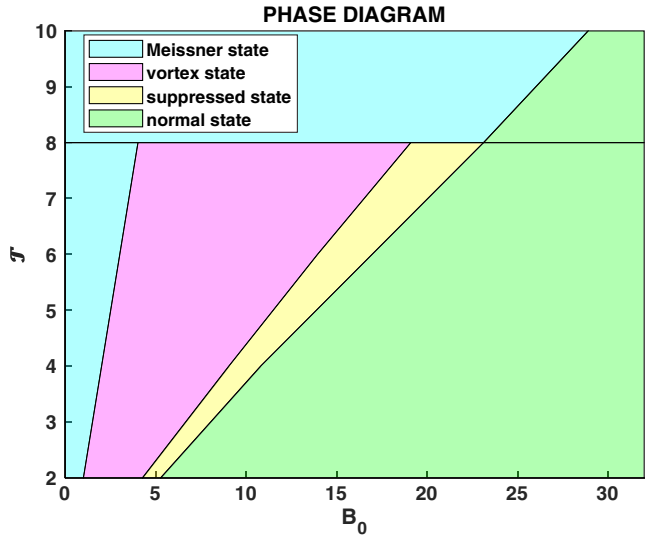

FIG. 7. The phase diagram of the holographic superconductor model with the magnetic period number ($\mathcal{T}$) on the x-axis and the strength of the magnetic field (B_0) on the y-axis. The cyan zone represents the meissner state in which magnetic field can not enter into superconductor. The magenta zone represents vortex state. The yellow zone represents suppressed state in which magnetic field suppressed order parameter for a long time, then the superconductor goes back to the vortex state or Meissner state. And the green zone represents normal state in which superconductor is completely destroyed by magnetic field.

V. SUMMARY

In this paper, we have presented a holographic superconductor model for the numerical investigation of the behavior of a superconducting film in response to a periodic magnetic field. Due to the back reaction of black hole is not considered, the dynamic equations was derived from the Lagrangian matter field $\mathcal{L}_{\text{matter}}(\Psi, A_\mu)$, the temperature and external magnetic field of the superconducting system were regulated by setting boundary conditions for the dynamic equations. When a periodic magnetic field interacts with the superconducting film within a suitable parameter range, patterns with multiple symmetries emerge, formed by vortex-antivortex pairs. This emergence results in both the effects of broken U(1) symmetry influenced by the magnetic field and a zero magnetic flux, attributable to the periodic features. The results exhibit diverse structures of vortex states, encompassing the Wigner crystallization state, the vortex cluster state, and the suppressed state, across different period numbers ($\mathcal{T}$) and magnetic field strengths (B_0). Through a series of simulations, it is observed that when the quantity

of vortices in the pattern is very small, the results are exactly the same for both large and medium-sized systems if the system scale increases by integer multiples. However, if the increase in system scale is not an integer multiple, the pattern may differ. Nevertheless, the symmetry remains constant when the magnetic period $\mathcal{T}$ is fixed in very large systems/medium-sized systems. On the other hand, when both the system scale and the magnetic period number are very large, the system becomes highly complex, and the symmetry may no longer be maintained. This observation is also evident in cases with a very small magnetic period number and medium-sized systems, as shown in Figs. 1(g)–(h). Due to this point, the phase diagram may vary with changes in the system scale. A larger system, allowing for a larger magnetic period number, introduces changes in the annihilation of vortices dependent on the gap between magnetic dots. With the scale of the system increasing and the gap growing larger while maintaining $\mathcal{T}$ fixed, the vortex pairs that would have been annihilated may no longer undergo annihilation. This leads to the emergence of a more complex phase diagram. In general, the symmetry of the patterns remains unaffected by the system scale, resulting in no qualitative distinctions observed in very large or medium-sized systems. Therefore, we have opted to maintain a fixed-system scale, treating it as a constant, while allowing the magnetic field and magnetic period to vary as variables. As the magnetic field increases, for $2 < \mathcal{T} < 8$, the superconductor undergoes transitions through the Meissner state, the vortex state (encompassing Wigner crystallization and vortex clusters), the suppressed state, and eventually reaches the normal state. If $\mathcal{T} > 8$, the superconductor will transition directly from the Meissner state to the normal state. We also provided a phase diagram with the period number ($\mathcal{T}$) and the strength of the magnetic field (B_0) to sum up the results. Finally, the observation can be verified since the experimental developments enabled to produce a periodic magnetic field with the magnetic cubic dot array on the top of superconductor directly [62–64].

ACKNOWLEDGMENTS

This work is supported by the National Natural Science Foundation of China (under Grants No. 11275233) and the Postgraduate Research and Practice Innovation Program Jiangsu Province (KYCX22_3450).

[1] G. Blatter, M. V. Feigel'man, V. B. Geshkenbein, A. I. Larkin, and V. M. Vinokur, Rev. Mod. Phys. **66**, 1125 (1994).
[2] P. G. de Gennes, *Superconductivity of Metals and Alloys* (Benjamin, New York, 1966).
[3] V. L. Ginzburg and L. D. Landau, On the theory of superconductivity, in *On Superconductivity and Superfluidity: A Scientific Autobiography* (Springer Berlin Heidelberg, Berlin, Heidelberg, 2009), pp. 113–137.
[4] B. Rosenstein and D. Li, Rev. Mod. Phys. **82**, 109 (2010).
[5] M. Tinkham, *Introduction to Superconductivity* (Dover Publication, Mineola, New York, 2004).
[6] E. H. Brandt, Rep. Prog. Phys. **58**, 1465 (1995).
[7] E. B. Bogomolny, Sov. J. Nucl. Phys. **24**, 449 (1976).
[8] L. Jacobs and C. Rebbi, Phys. Rev. B **19**, 4486 (1979).
[9] A. N. Bogdanov and D. A. Yablonskii, Zh. Eksp. Teor. Fiz. **95**, 178 (1989).
[10] A. J. Beekman and J. Zaanen, Front. Phys. **6**, 357 (2011).
[11] R. Geurts, M. V. Milošević, and F. M. Peeters, Phys. Rev. B **81**, 214514 (2010).
[12] A. A. Shanenko, M. V. Milošević, F. M. Peeters, and A. V. Vagov, Phys. Rev. Lett. **106**, 047005 (2011).
[13] A. Vagov, S. Wolf, M. D. Croitoru, and A. Shanenko, Commun. Phys. **3**, 58 (2020).
[14] A. A. Abrikosov, Sov. Phys. JETP **5**, 1174 (1957).
[15] J. K. Hulm, Science **154**, 1634 (1966).
[16] A. Jacobs, Canadian J. Phys. **60**, 299 (1982).
[17] G. Blatter, M. V. Feigel'man, V. B. Geshkenbein, A. I. Larkin, and V. M. Vinokur, Rev. Mod. Phys. **66**, 1125 (1994).
[18] B. Rosenstein and D. Li, Rev. Mod. Phys. **82**, 109 (2010).
[19] M. V. Milošević and F. M. Peeters, Phys. Rev. B **68**, 024509 (2003).
[20] M. V. Milošević and F. M. Peeters, Phys. Rev. Lett. **93**, 267006 (2004).
[21] M. V. Milošević and F. M. Peeters, Phys. Rev. Lett. **94**, 227001 (2005).
[22] R. Geurts, M. V. Milošević, and F. M. Peeters, Phys. Rev. Lett. **97**, 137002 (2006).
[23] G. R. Berdiyorov, M. V. Milošević, and F. M. Peeters, Phys. Rev. Lett. **96**, 207001 (2006).
[24] G. R. Berdiyorov, M. V. Milošević, and F. M. Peeters, Phys. Rev. B **79**, 184506 (2009).
[25] E. Witten, Adv. Theor. Math. Phys. **2**, 253 (1998).
[26] S. S. Gubser, I. R. Klebanov, and A. M. Polyakov, Phys. Lett. B **428**, 105 (1998).
[27] J. Maldacena, Int. J. Theor. Phys. **38**, 1113 (1999).
[28] S. S. Gubser, Phys. Rev. D **78**, 065034 (2008).
[29] S. A. Hartnoll, C. P. Herzog, and G. T. Horowitz, Phys. Rev. Lett. **101**, 031601 (2008).
[30] Paul Wittmer, Christian-Marcel Schmied, Thomas Gasenzer, and Carlo Ewerz, Phys. Rev. Lett. **127**, 101601 (2021).
[31] Mario Flory, Sebastian Grieninger, and Sergio Morales-Tejera, arXiv:2209.09251.

[32] Yu-Kun Yan, Shanquan Lan, Yu Tian, Peng Yang, Shunhui Yao, and Hongbao Zhang, Phys. Rev. D **107**, L121901 (2023).
[33] Peng Yang, Matteo Baggioli, Zi Cai, Yu Tian, and Hongbao Zhang, Phys. Rev. Lett. **131**, 221601 (2023).
[34] Shanquan Lan, Xin Li, Yu Tian, Peng Yang, and Hongbao Zhang, Phys. Rev. Lett. **131**, 221602 (2023).
[35] Irene Amado, Matthias Kaminski, and Karl Landsteiner, J. High Energy Phys. 05 (2009) 021.
[36] Jyotirmoy Bhattacharya, Sayantani Bhattacharyya, and Shiraz Minwalla, J. High Energy Phys. 04 (2011) 125.
[37] Daniel Arean, Matteo Baggioli, Sebastian Grieninger, and Karl Landsteiner, J. High Energy Phys. 11 (2021) 206.
[38] C.-Y. Xia, H.-B. Zeng, H.-Q. Zhang, Z.-Y. Nie, Y. Tian, and X. Li, Phys. Rev. D **100**, 061901(R) (2019).
[39] X. Li, Y. Tian, and H. Zhang, J. High Energy Phys. 02 (2020) 104.
[40] J.-H. Su, C.-Y. Xia, W.-C. Yang, and H.-B. Zeng, Phys. Rev. D **107**, 026006 (2023).
[41] T. Albash and C. V. Johnson, J. High Energy Phys. 09 (2008) 121.
[42] T. Albash and C. V. Johnson, arXiv:0906.0519.
[43] E. Nakano and W.-Y. Wen, Phys. Rev. D **78**, 046004 (2008).
[44] M. Natsuume and T. Okamura, Phys. Rev. D **106**, 086005 (2022).
[45] M. Baggioli, J. Hologr. Appl. Phys. **3**, 2 (2023).
[46] M. Baggioli, K.-B. Huh, H.-S. Jeong, K.-Y. Kim, Y.-W. Sun, J. High Energy Phys. 02 (2023) 012.
[47] H.-S. Jeong, M. Baggioli, K.-Y. Kim, and Y.-W. Sun, J. High Energy Phys. 03 (2023) 206.
[48] M. Montull, A. Pomarol, and P. J. Silva, Phys. Rev. Lett. **103**, 091601 (2009).
[49] O. Domenech, M. Montull, A. Pomarol, A. Salvio, and P. J. Silva, J. High Energy Phys. 08 (2010) 033.
[50] V. Keränen, E. Keski-Vakkuri, S. Nowling, and K. P. Yogendran, Phys. Rev. D **81**, 126012 (2010).
[51] T. Albash and C. V. Johnson, Phys. Rev. D **80**, 126009 (2009).
[52] K. Maeda, M. Natsuume, and T. Okamura, Phys. Rev. D **81**, 026002 (2010).
[53] A. Donos, J. P. Gauntlett, and C. Pantelidou, J. High Energy Phys. 07 (2020) 095.
[54] C.-Y. Xia, H.-B. Zeng, Y. Tian, C.-M. Chen, and J. Zaanen, Phys. Rev. D **105**, L021901 (2022).
[55] B. Withers, J. High Energy Phys. 09 (2014) 102.
[56] A. Donos, J. P. Gauntlett, J. Sonner, and B. Withers, J. High Energy Phys. 03 (2013) 108.
[57] Sean A. Hartnoll, Christopher P. Herzog, and Gary T. Horowitz, J. High Energy Phys. 12 (2008) 015.
[58] C. P. Herzog, P. K. Kovtun, and D. T. Son, Phys. Rev. D **79**, 066002 (2009).
[59] K. Skenderis, Classical Quantum Gravity **19**, 5849 (2002).
[60] E. Witten, SL(2,Z) action on three-dimensional conformal field theories with Abelian symmetry, in *From Fields to Strings*, edited by M. Shifman *et al.* (E. Witten, Singapore, 2005), Vol. 2, pp. 1173–1200.
[61] O. Domenech, M. Montull, A. Pomarol, A. Salvio, and P. J. Silva, J. High Energy Phys. 08 (2010) 033.
[62] L. F. Chibotaru, A. Ceulemans, V. Bruyndoncx, and V. V. Moshchalkov, Nature (London) **408**, 833 (2000).
[63] M. Lange, M. J. Van Bael, Y. Bruynseraede, and V. V. Moshchalkov, Phys. Rev. Lett. **90**, 197006 (2003).
[64] J. del Valle, A. Gomez, J. Luis-Hita, V. Rollano, E. M. Gonzalez, and J. L. Vicent, Supercond. Sci. Technol. **30**, 025014 (2016).
[65] K. Epstein, A. M. Goldman, and A. M. Kadin, Phys. Rev. Lett. **47**, 534 (1981).
[66] See Supplemental Material at http://link.aps.org/supplemental/10.1103/PhysRevD.109.046019 for the video of dynamic process of the suppressed state formation and reverts to the meissner state when $\mathcal{T} = 4$, $A_0 = 38$, $B_0 = 9.5504$ and $T = 0.406T_c$, and also to the vortex state when $\mathcal{T} = 2$, $A_0 = 38$, $B_0 = 4.7752$ and $T = 0.406T_c$.